Available online at www.eccomasproceedia.org
Eccomas Proceedia COMPDYN (2017) 4358-4373

ECCOMAS
Proceedia

COMPDYN 2017
6th ECCOMAS Thematic Conference on
Computational Methods in Structural Dynamics and Earthquake Engineering
M. Papadrakakis, M. Fragiadakis (eds.)
Rhodes Island, Greece, 15–17 June 2017

COMPARISON OF FRICTION MODELS FOR THE CURVED SURFACE SLIDING SYSTEM IN THE NONLINEAR SEISMIC ANALYSIS OF BASE-ISOLATED BUILDINGS

F. Mazza[1] **and M. Loprete**[2]

[1] Dipartimento di Ingegneria Civile, Università della Calabria
Via P. Bucci, 87036 Rende (CS), Italy
e-mail: fabio.mazza@unical.it

[2] Dipartimento di Ingegneria Civile, Università della Calabria
Via P. Bucci, 87036 Rende (CS), Italy
mattia_loprete@outlook.com

Keywords: R.C. Base-isolated Structure; Curved Surface Sliding System; Sliding Velocity; Axial Pressure; Stick-Slip Effect; Axial Load; Temperature; Nonlinear Dynamic Analysis.

Abstract. *Current seismic codes allow for the use of simple bilinear curves to describe the nonlinear response of the curved surface sliding (CSS) bearings. However, the CSS bearings show a complex nonlinear behavior with variations in the friction coefficient, depending on the sliding velocity, axial pressure, heating at the sliding surface and stick-slip phases at the initial motion and motion reversals. Moreover, the friction force and lateral stiffness during the sliding phase are proportional to the axial load. The main object of this study is to investigate the influence that different modelling assumptions of the CSS bearings may have on the lateral-torsional response of irregular base-isolated structures located in near-fault area, characterized by ground motions with large amplitudes and long period horizontal velocity pulses. To this end, a six-storey base-isolated reinforced concrete (r.c.) framed building, with an L-shaped plan and setbacks in elevation, is designed assuming low- and medium-type friction properties, both with two in-plan distributions of the dynamic-fast friction coefficient, corresponding to: (i) the same value for all isolators; (ii) a different value for each isolator. Four additional cases are compared reducing the friction coefficient in accordance with a temperature increase up to 250°C during ground motions. A computer code for the nonlinear dynamic analysis, with a lumped plasticity model to describe the inelastic behaviour of the superstructure, is developed in order to compare eight structural solutions through five models of the CSS bearings that consider: i) constant axial load and constant friction coefficient; ii) constant axial load and variable friction coefficient with velocity; iii) variable axial load and variable friction coefficient with velocity; iv) variable axial load and variable friction coefficient with velocity and pressure; v) variable axial load and variable friction coefficient with velocity, pressure and stick-slip effect. To this end, near-fault ground motions are selected from the Pacific Earthquake Engineering Research center database.*

Peer-review under responsibility of the organizing committee of COMPDYN 2017.
doi: 10.7712/120117.5729.17328

1 INTRODUCTION

Curved surface sliding (CSS) bearings are generally recommended for irregular framed structures because, in comparison with other base-isolation systems, allow the minimization of torsional effects and residual displacements [1]. More specifically, mass irregularities of the superstructure are balanced by spatial variation in the horizontal stiffness and friction force of the CSS bearings, proportional to the axial load during the sliding phase. However, theoretical and experimental studies have uncovered the complex nonlinear behaviour of the CSS bearings, highlighting the presence of many parameters affecting their friction coefficient at the sliding surface. More specifically, the friction force changes with: (a) the sliding velocity, whose increasing values produce a friction coefficient which increases by an exponential law [2]; (b) the axial pressure, with a high-velocity (dynamic-fast) value of the friction coefficient significantly reducing with the axial pressure and a low-velocity (dynamic-low) value which is relatively unaffected [3, 4]; (c) the temperature when the slider is in motion, influencing the friction coefficient which decreases rapidly as the temperature at the sliding interface increases from -40 °C to 20°C and trends to a constant value for temperatures greater than 250 °C [5]; (d) the stick-slip phases, producing a transition between static and kinetic friction coefficients, whose ratio varies between 1.5 and 4.5 depending on the friction material adopted to coat the slider [6]. On the other hand, the axial load changes continuously during an earthquake and high values of the sliding velocity are expected under the horizontal components of near-fault ground motions, thus inducing torsional effects and residual displacements of the CSS system [7-9]. These considerations show the need for a suitable numerical model to describe the nonlinear behaviour of a CSS bearing, contrary to current international seismic codes [10] and guidelines [11] which allow for the use of simple bilinear curves to reduce the computational effort for the nonlinear dynamic analyses.

To this end, a computer code for the nonlinear dynamic analysis is developed, in order to compare five models of the CSS bearings that consider: i) constant axial load and constant friction coefficient (CALCFC model); ii) constant axial load and variable friction coefficient with velocity (CALVFC1 model); iii) variable axial load and variable friction coefficient with velocity (VALVFC1 model); iv) variable axial load and variable friction coefficient with velocity and pressure (VALVFC2 model); v) variable axial load and variable friction coefficient with velocity, pressure and stick-slip effect (VALVFC3 model). A numerical investigation is carried out considering a six-storey reinforced concrete (r.c.) office building, with an L-shaped plan and setbacks at different heights along the in-plan X (i.e. one setback, at the third-storey) and Y (i.e. two setbacks, at the second- and fourth-storey) principal directions, designed in line with the Italian seismic code [12]. Eight structural solutions are compared, assuming: i) low- and medium-type friction properties; ii) two in-plan distributions of the dynamic-fast friction coefficient (i.e. the same value for all isolators and a different value for each isolator); iii) a reduction of the friction coefficient in accordance with a temperature increase up to 250°C during ground motions. A lumped plasticity model describes the inelastic behaviour of the superstructure, including a 26-flat surface modelling of the axial load-biaxial bending moment elastic domain at the end sections of r.c. frame members. Seven near-fault ground motions are selected from the *Pacific Earthquake Engineering Research center database* [13] and normalized in accordance with the design hypotheses adopted for the test structure (i.e. high-risk seismic region and soil-site).

2 MODELLING OF THE CURVED SURFACE SLIDING BEARING

The CSS bearing consists of a spherical concave sliding surface, with a radius of curvature R, and an articulated slider, with contact surface S and friction coefficient μ. For bidirectional

motion, the restoring force during the sliding phase contains pendular ($\boldsymbol{F}_p$) and friction ($\boldsymbol{F}_f$) components that can be evaluated by considering the rotational equilibrium equation around the centre of curvature [14]

$$\boldsymbol{F}_H = \boldsymbol{F}_p + \boldsymbol{F}_f = \begin{Bmatrix} F_{H,x} \\ F_{H,y} \end{Bmatrix} \cong \frac{N}{R} \begin{Bmatrix} u_{H,x} \\ u_{H,y} \end{Bmatrix} + \mu N \frac{1}{\|\dot{u}_H\|} \begin{Bmatrix} \dot{u}_{H,x} \\ \dot{u}_{H,y} \end{Bmatrix} \tag{1}$$

where N is the axial load on the CSS bearing corresponding to the axial pressure $p=N/S$. Moreover, a circular interaction domain can be used to represent the biaxial interaction, where the direction of the hysteretic force is controlled by the incremental plastic displacements [15].

2.1 CALCFC model: constant axial load and constant friction coefficient

The response of the CSS bearing in the horizontal direction can be idealized by means of a two-component model (Figure 1a), constituted of an elastic component with restoring stiffness $K_r=N/R$ and an elastic-plastic component with elastic stiffness K_i-K_r and yield force μW. A bilinear force-displacement ($\boldsymbol{F}_H$-$\boldsymbol{u}_H$) law (Figure 2b) can be assumed for constant values of the axial load (i.e. $N=W$, W being the weight of the superstructure) and friction coefficient μ. It should be noted that the initial stiffness K_i takes into account the slight deformation (i.e. $\boldsymbol{u}_{Hi}\cong 0.5$ mm) at the sliding surface during the stick phase [16].

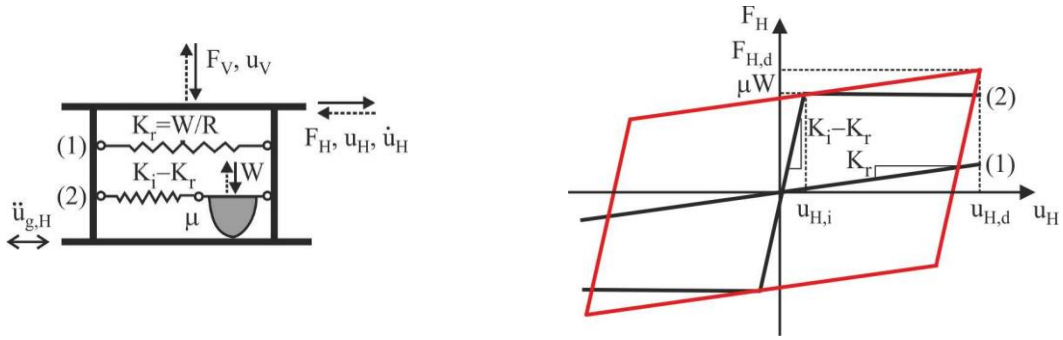

(a) (b)

Figure 1: CALCFC model for a CSS bearing.

2.2 CALVFC1 model: constant axial load and variable friction coefficient with velocity

The instantaneous sliding velocity affects the friction force of a CSS bearing (Figure 2), with a monotonic increase with the sliding velocity up to a constant value [2].

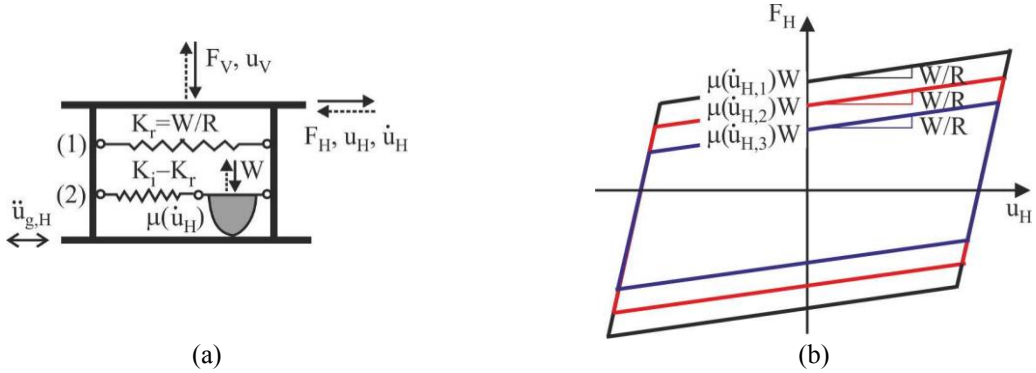

(a) (b)

Figure 2: CALVFC1 model for a CSS bearing.

An exponential law can describe the velocity dependence of the friction coefficient [2]:

$$\mu(\dot{u}_H) = \mu_{fast} - (\mu_{fast} - \mu_{slow}) e^{-\alpha \dot{u}_H} \tag{2}$$

where μ_{slow} and μ_{fast} are the friction coefficients at low and fast sliding velocities, respectively, and α is a rate parameter which depends on the axial load and condition of the interface. In particular, experimental results indicate that the dynamic-slow friction coefficient can be assumed 2.5 times lower than μ_{fast} [17], while parameter α can be considered equal to approximately 0.1 s/mm [5].

2.3 VALVFC1 model: variable axial load and variable friction coefficient with velocity

At any given moment during an earthquake, the fluctuation in the bearing axial load produces changes in $\boldsymbol{F}_f$ and K_r (Figure 3). The axial load acting on a CSS bearing can be modified in accordance with the following expression which also accounts for the vertical-horizontal coupling [18]

$$N = W\left(1 + \frac{N_{OM}}{W}\right) \tag{3}$$

where N_{OM} is the additional axial load, positive when compressive, due to the overturning moment produced by the horizontal ground acceleration $\ddot{u}_{g,H}$ (Figure 3a).

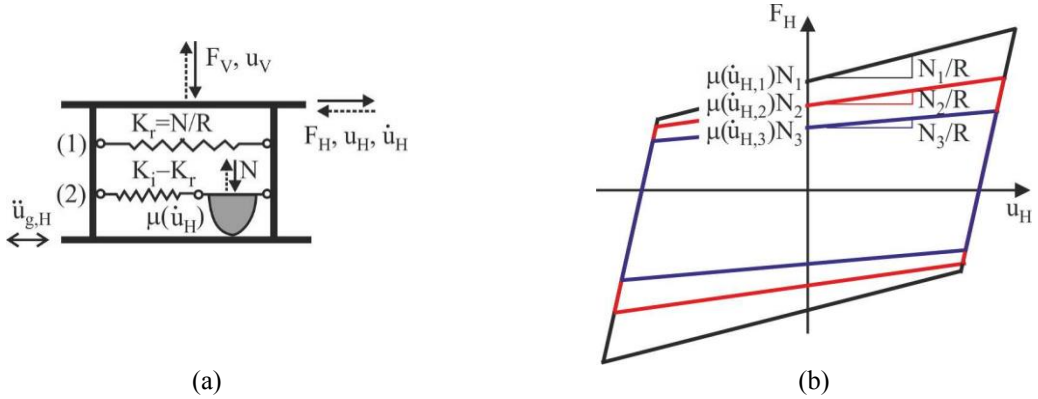

Figure 3: VALVFC1 model for a CSS bearing.

Furthermore, the CSS bearing does not resist tensile axial loads and it is thus free to uplift. A gap element with infinitely rigid behaviour in compression is assumed in the vertical direction, to consider the fact that the reversal of the axial load from compression to tension is possible

$$F_V = N \quad \text{for } u_V \geq 0 \text{ and } F_V = 0 \quad \text{for } u_V < 0 \tag{4}$$

where the equivalent viscous damping in the vertical direction is neglected.

2.4 VALVFC2 model: variable axial load and variable friction coefficient with velocity and pressure

The instantaneous pressure due to the axial load affects the friction coefficient of a CSS bearing (Figure 4), with a reduction of μ_{fast} for increasing values of axial load, while the dependence of μ_{slow} and α on the axial load can be neglected [3]. Experimental laws can be assumed to take into account the variability of the dynamic-fast friction coefficient with the axial pressure [4], assuming low-

$$\mu_{fast,LF}(\%) = 2.5\left(\frac{p_{Sd}}{p_{Ed}}\right)^{-0.834} \text{ for } \left(\frac{p_{Sd}}{p_{Ed}}\right) > 0.1;\ \mu_{fast,LF}(\%) = 17 \text{ for } \left(\frac{p_{Sd}}{p_{Ed}}\right) \le 0.1 \quad (5a,b)$$

and medium-type

$$\mu_{fast,MF}(\%) = 5.5\left(\frac{p_{Sd}}{p_{Ed}}\right)^{-0.563} \text{ for } \left(\frac{p_{Sd}}{p_{Ed}}\right) > 0.135;\ \mu_{fast,MF}(\%) = 17 \text{ for } \left(\frac{p_{Sd}}{p_{Ed}}\right) \le 0.135 \quad (6a,b)$$

friction properties, where p_{Ed} and p_{Sd} represent, respectively, the maximum axial pressure capacity and the quasi-permanent gravity pressure ($p_{Sd}=p_v$) evaluated in the CSS system.

Then, a modified expression of the friction law can be formulated:

$$\mu(\dot{u}_H, p) = k_p\left[\mu_{fast} - \left(\mu_{fast} - \mu_{slow}\right)e^{-\alpha\dot{u}_H}\right] \quad (7)$$

where the modification factor

$$k_p = \mu_{fast}(p)/\mu_{fast}(p_v) \quad (8)$$

is defined as ratio between the dynamic-fast friction coefficient during the motion and corresponding value at the reference axial pressure under gravity loads (p_v).

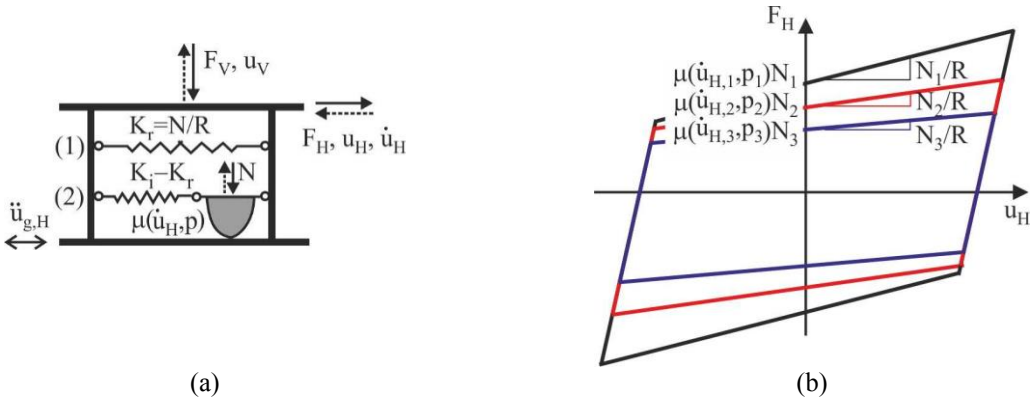

Figure 4: VALVFC2 model for a CSS bearing.

2.5 VALVFC3 model: variable axial load and variable friction coefficient with velocity, pressure and stick-slip effect

At initial motion and motion reversals, the response of the CSS bearing shifts between sticking and sliding phases highlighting a static friction coefficient greater than the dynamic one (Figure 5).

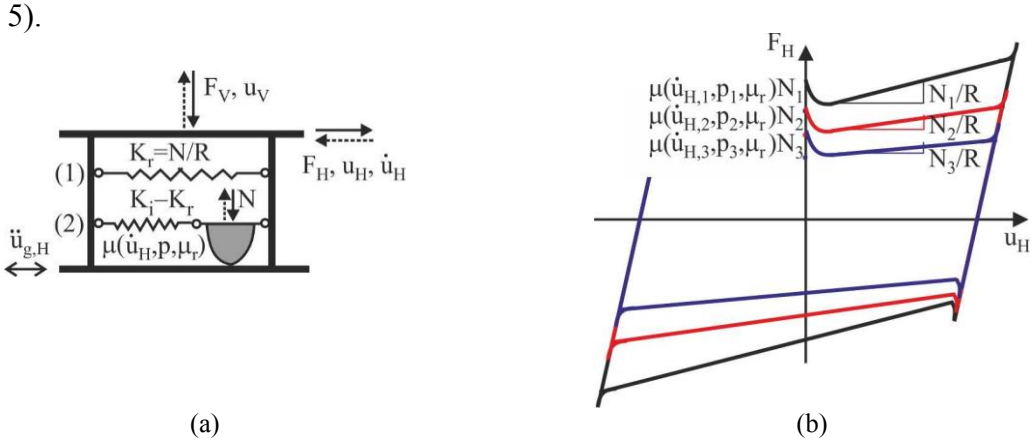

Figure 5: VALVFC3 model for a CSS bearing.

In particular, initial sliding occurs when the frictional force, depending on the breakaway friction coefficient (μ_b), is overcome. Moreover, an increase of the lateral force can be observed when the maximum displacement is reached, corresponding to the friction coefficient at motion reversal (μ_r). In order to take into account the transition between the sliding and sticking phase, the following simplified expression can be used

$$\mu(\dot{u}_H, p, \mu_b, \mu_r) \cong \mu(\dot{u}_H, p, \mu_r) = k_p \left[\mu_{fast} - (\mu_{fast} - \mu_r) e^{-c\dot{u}_H} \right] \tag{9}$$

where the dynamic-slow friction coefficient (μ_{min}) is replaced with the static value at motion reversal (μ_r) and $\mu_r \cong \mu_b$ is assumed, so observing that the breakaway friction coefficient disappears after one cycle of loading [6]. A ratio $\mu_r/\mu_{max} \cong 2$ and a parameter $c \cong \alpha$ are also assumed [6].

3 TEST STRUCTURES AND SELECTED EARTHQUAKES

Eight six-storey base-isolated r.c. framed office buildings, irregular in plan (Figure 6a) and elevation (Figures 6b,c), are designed in line with the Italian seismic code (NTC08, [12]). The following assumptions are considered to evaluate the horizontal seismic loads: elastic response of the superstructure (i.e. behaviour factor q_H=1); soil site (i.e. subsoil class D); high risk seismic region (i.e. peak ground accelerations: PGA_{LS}=0.27gx1.416=0.382g, at the life-safety limit state for the superstructure; PGA_{CP}=0.36gx1.061=0.382g, at the collapse prevention limit state for the base-isolation system). The gravity loads used in the design are represented by a dead load of 6.7 kN/m^2 and a live load of 2.0 kN/m^2, on all floors. Masonry infill walls of 2.7 kN/m^2 are considered as nonstructural elements regularly distributed along the perimeter and in elevation. The design of the superstructure is carried out in compliance with the life-safety limit state. Detailing for local ductility is also imposed to satisfy minimum conditions for the longitudinal bars of the r.c. frame members. A cylindrical compressive strength of 25 N/mm^2 for the concrete and a yield strength of 450 N/mm^2 for the steel are assumed for the r.c. frame members. Cross sections of columns and beams along the in-plan X and Y directions are reported in Tables 1 and 2, respectively. Further details can be found in a previous work [19].

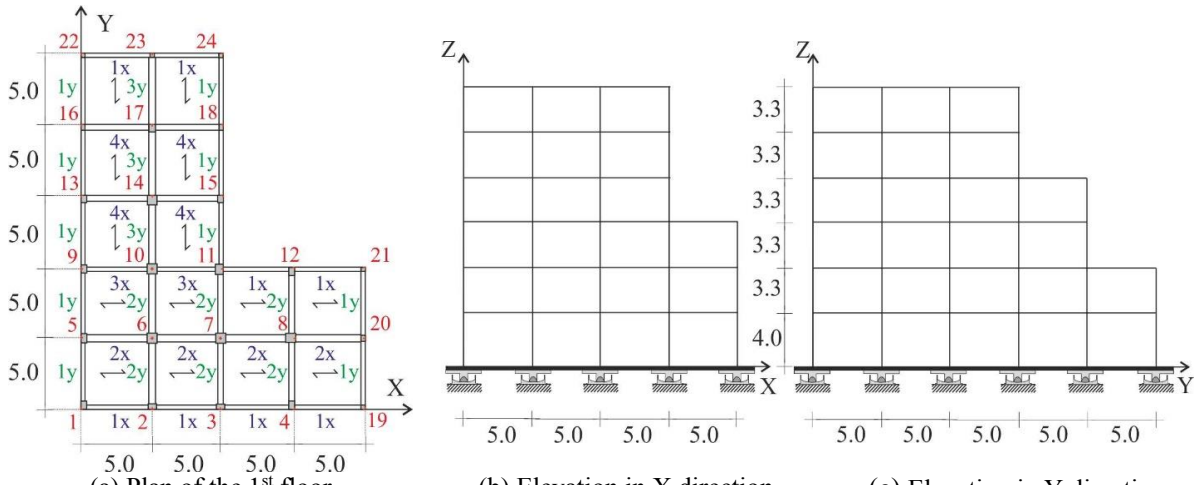

(a) Plan of the 1st floor (b) Elevation in X direction (c) Elevation in Y direction

Figure 6: Base-isolated r.c. test structure (units in m).

A grid of rigid beams is placed at the base of the framed structure on the single CSS system. The FP system is designed at the CP limit state, requiring the fulfilment of the provisions

imposed by NTC08: i.e. maximum compression axial load of the FP bearing less than its capacity; maximum horizontal displacements less than the spectral value; absence of tensile axial loads at the level of the FP system.

	Storey					
Column	1	2	3	4	5	6
1	40×60	35×55	30×50	30×45	30×40	30×35
2	60×40	50×35	50×30	40×30	30×30	30×30
3	60×40	50×35	50×30	40×30	30×30	30×30
4	40×60	35×55	30×50	30×45	30×40	30×35
5	40×60	35×50	35×40	30×40	30×30	30×30
6	70×70	65×65	60×60	50×50	40×40	30×30
7	70×70	65×65	60×60	50×50	40×40	30×30
8	60×60	55×55	50×50	45×40	40×30	35×30
9	40×60	35×50	30×50	30×40	30×30	30×30
10	70×70	65×65	60×60	50×50	40×40	30×30
11	55×70	50×65	45×60	40×50	35×40	30×30
12	40×60	35×55	30×50	30×45	30×40	30×35
13	40×50	35×50	30×40	30×35	30×30	30×30
14	65×65	60×60	50×50	45×45	35×40	30×35
15	40×50	35×45	30×40	30×35	30×30	30×30
16	30×40	30×35	30×30	30×30	-	-
17	50×50	45×45	35×40	30×35	-	-
18	30×40	30×35	30×30	30×30	-	-
19	30×30	30×30	30×30	-	-	-
20	30×40	30×35	30×30	-	-	-
21	30×30	30×30	30×30	-	-	-
22	30×30	30×30	-	-	-	-
23	35×30	30×30	-	-	-	-
24	30×30	30×30	-	-	-	-

Table 1: Cross-sections of r.c. columns (units in cm).

	Floor					
Beam	1	2	3	4	5	6
1x	30×60	30×60	30×60	30×60	30×60	30×60
2x	50×21	50×21	50×21	50×21	50×21	50×21
3x	30×55	30×55	30×55	30×55	30×55	30×55
4x	40×65	40×65	40×65	40×65	-	-
1y	30×60	30×60	30×60	30×60	30×60	30×60
2y	40×65	40×65	40×65	40×65	40×65	40×65
3y	50×21	50×21	50×21	50×21	50×21	50×21

Table 2: Cross-sections of r.c. beams (units in cm).

Starting from the fundamental vibration period and equivalent viscous damping

$$T_{e,I} = 2\pi \sqrt{\left[g\left(\frac{1}{R} + \frac{\mu_{fast}}{u_{H,d}} \right) \right]^{-1}} \quad ; \quad \xi_{e,I} = \frac{2}{\pi} \frac{1}{1 + \dfrac{u_{H,d}}{\mu_{fast} R}} \tag{10a,b}$$

with effective values equal to 3s and 15%, respectively, the values of the radius of curvature (R=2.93 m) and dynamic-fast friction coefficient (μ_{fast}= 4.2%) of the CSS system are evaluated in relation to the spectral displacement $u_{H,d}$= 0.394 m at the collapse prevention limit state. In the case of low friction, the maximum axial load capacity of the CSS bearings

(N_{Ed}) is evaluated by Equations (5a,b), as function of the assigned value of the quasi-permanent gravity loads (N_{Sd}) transmitted from the superstructure. Then, in the case of medium friction, the friction coefficient corresponding to the same ratio N_{Sd}/N_{Ed} is obtained by Equations (6a,b). Moreover, two in-plan distributions of N_{Ed} are assumed for the base-isolated structures: BIA.LF and BIA.MF structures in Figure 7a, with fifteen types of friction pendulum (FP) bearings (i.e. having the same μ_{fast} value for all isolators); BIB.LF and BIB.MF structures in Figure 7b, with only three types of FP bearings (i.e. exhibiting different μ_{fast} value for each isolator), which are selected with reference to the maximum value of N_{Ed} from those of the isolators corresponding to three ranges of $\beta=N_{Sd}/N_{Sd,max}$ (i.e. $\beta\leq0.4$; $0.4<\beta\leq0.7$; $\beta>0.7$).

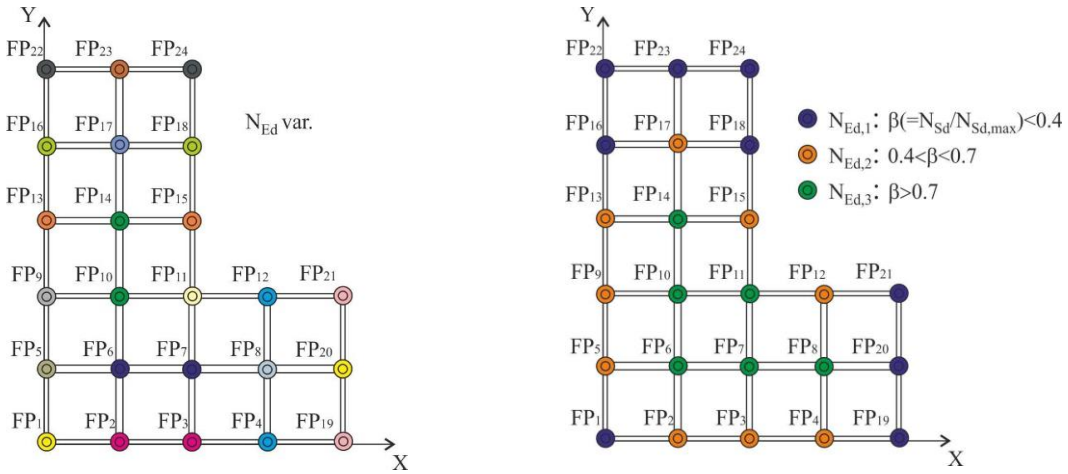

(a) BI.AL and BI.AM structures: n.15 FP. (b) BI.BL and BI.BM structures: n.3 FP.

Figure 7: In-plan distributions of axial load capacity for the Friction Pendulum (FP) bearings.

Thereafter, four additional structures are designed for low- (i.e. BIA.LFT and BIB.LFT) and medium-type (i.e. BIA.MFT and BIB.MFT) friction properties by taking into account the dependence of the dynamic-fast friction coefficient on the heating at the sliding surface when the slider is in motion. To this end, a reduction factor k_T of the friction coefficient [5]

$$k_{Tf}=\frac{\mu_{fast,T_f}}{\mu_{fast}}=0.79\left(0.7^{0.02T_f}+0.4\right) \tag{11}$$

is applied to the Equations (5a,b) and (6a,b). It is worth noting that the reduction in the friction coefficient is sudden for increasing temperature from T_f=–40 °C to T_f=20 °C and trends to a constant value for temperatures greater than T_f=250 °C, where a reduction factor equal to 0.45 is obtained. Design parameters of the CSS systems are reported in Table 3.

	BIA.LF	BIB.LF	BIA.MF	BIB.MF	BIA.LFT	BIB.LFT	BIA.MFT	BIB.MFT
T_{eI}	2.96	2.89	2.45	2.41	3.08	3.04	3.07	3.02
ξ_{eI} (%)	16	18	31	32	12	13	13	14
$u_{H,d}$	0.376	0.352	0.252	0.246	0.429	0.416	0.423	0.404
T_f	20	20	20	20	250	250	250	250
FP types	15	3	15	3	15	3	15	3

Table 3: Design parameters of the CSS systems (units in s, m and °C).

Horizontal components of seven near-fault earthquakes characterized by long-duration velocity pulses are selected from the *Pacific Earthquake Engineering Research center database* [13], on the basis of the design hypotheses adopted for the test structures (i.e. soil site and

high risk seismic region). In Table 4 the main data of the selected near-fault ground motions are shown: i.e. year; recording station; magnitude (M_w); distance from the fault (Δ); pulse period (T_P); peak ground acceleration for the two horizontal components (i.e. PGA_{H1} and PGA_{H2}). The elastic response spectra of velocity ($S_{v,H}$) for the two horizontal components of each ground motion are plotted in Figure 8, assuming an equivalent viscous damping ratio in the horizontal direction (ξ_H) of 15%. These response spectra are compared with the corresponding NTC08 response spectra for a high-risk seismic region and subsoil class D (i.e. soil site), considering the collapse prevention limit state.

Earthquake	Recording station	M_w	Δ [km]	T_p [s]	PGA_{H1}	PGA_{H2}
Chi-Chi, 1999	TCU068	7.6	0.3	12.29	0.566 g	0.462 g
Imperial Valley, 1979	El Centro D.A.	6.5	5.1	6.27	0.353 g	0.481 g
Kobe,1995	Takatori	6.9	1.5	1.55	0.618 g	0.671 g
Loma Prieta, 1989	Gilroy #3	6.9	12.8	2.64	0.559 g	0.368 g
Northridge, 1994	Rinaldi R.S.	6.7	6.5	1.25	0.874 g	0.472 g
Parkfield, 2004	Fault Zone 1	6.0	2.5	1.19	0.605 g	0.833 g
Superstition H., 1987	Parachute T.S.	6.5	1.0	2.39	0.432 g	0.384 g

Table 4: Main data of the selected near-fault ground motions.

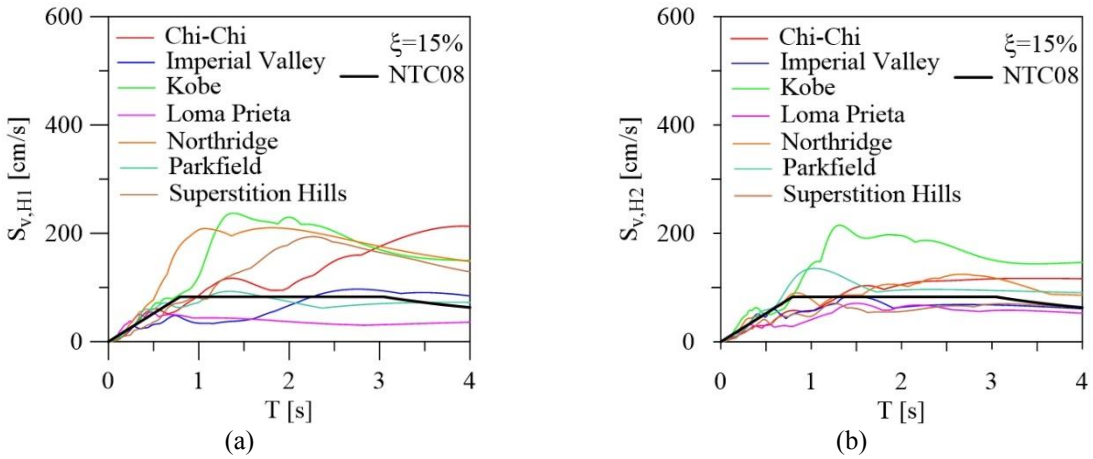

Figure 8: Velocity (elastic) response spectra for the horizontal components of the selected earthquakes.

Note that within the range of quite long horizontal vibration periods (i.e. $T_I \geq 2.4$s), corresponding to the base-isolated test structures, $S_{v,H}$ values for the selected motions are considerably different from those of the corresponding NTC08 design spectrum. Thus, the choice of the *Modified Velocity Spectrum Intensity* (*MVSI*) for scaling real motions [20]

$$MVSI = \int_{0.5T}^{1.25T} S_v(T,\xi) \cdot dT \tag{12}$$

being T the fundamental vibration period of the base-isolated structure. Then, the scale factor (*SF*), whereby the horizontal components of the selected real accelerograms are normalized with respect to the NTC08 ones, is calculated as

$$SF_{MVSI} = \int_{0.5T}^{1.25T} S_{v,NTC08}(T,\eta) \cdot dT \Bigg/ \left[0.5 \left(\int_{0.5T}^{1.25T} S_{v1,NF}(T,\xi) \cdot dT + \int_{0.5T}^{1.25T} S_{v2,NF}(T,\xi) \cdot dT \right) \right] \tag{13}$$

Scale factors of the selected near-fault earthquakes are reported in Table 5.

Structure	TCU068	El Centro	Takatori	Gilroy #3	Rinaldi R.S.	Fault Zone 1	Parachute T.S.
BIA.LF	0.58	1.00	0.49	1.70	0.59	1.05	0.71
BIB.LF	0.58	0.99	0.48	1.67	0.59	1.03	0.70
BIA.MF	0.63	0.97	0.46	1.45	0.55	0.90	0.69
BIB.MF	0.64	0.97	0.45	1.43	0.54	0.89	0.70
BIA.LFT	0.57	1.04	0.50	1.77	0.61	1.09	0.72
BIB.LFT	0.58	1.03	0.49	1.75	0.61	1.08	0.72
BIA.MFT	0.57	1.03	0.49	1.76	0.61	1.08	0.72
BIB.MFT	0.57	1.02	0.49	1.74	0.60	1.07	0.72

Table 5: Scale factors of the selected near-fault ground motions.

4 NUMERICAL RESULTS

Nonlinear dynamic analyses of eight structural solutions are carried out to evaluate the effects of different modelling and design assumptions of CSS bearings on the seismic response of irregular r.c. base-isolated structures subjected to strong near-fault ground motions. For this purpose, five models of CSS bearings, that consider constant and variable axial load combined with constant and variable friction coefficient, are compared for the CSS base-isolation system. A lumped plasticity model comprising two parallel elements, one linearly elastic and the other elastic-perfectly plastic, is used to describe the inelastic behaviour of r.c. frame members of the superstructure [21]. A piecewise linearization of the axial load-biaxial bending moment ultimate domain is considered for r.c. cross-sections [22]. Moreover, a stiffness-proportional damping matrix of the superstructure is considered, by applying a viscous damping ratio ξ_S=1% to the fundamental vibration period of the base-isolated structures [8]. The results discussed below are evaluated as an average of those separately obtained for each set of seven near-fault earthquakes scaled in accordance to MVSI [20].

First, three demand parameters are evaluated at the level of the CSS system: i) maximum bearing displacement ($u_{BI,max}$), representing a measure of the damage at the isolation level; residual bearing displacement ($u_{BI,res}$), related to the re-centring capability of the CSS bearings; iii) in-plan drift ratio $(tg\theta)_{BI,max}$ evaluated as the in-plan relative displacement of the CSS system divided by the length of the building plan, which is an indicator of the displacement due to torsion. In particular, five nonlinear models of the CSS bearings are compared at an ambient temperature T=20 °C (i.e. CALCFC, CALVFC1, VALVFC1, VALVFC2 and VALVFC3). Moreover, two in-plan distributions of dynamic-fast friction coefficient for the CSS system (i.e. BIA and BIB structures) are examined in Figures 9-11, considering low- (i.e. BIA.LF and BIB.LF) and medium-type (i.e. BIA.MF and BIB.MF) friction properties of the CSS bearings.

As shown in Figure 9, similar values of maximum bearing displacement are obtained in all the examined cases where constant (i.e. CAL) and variable (i.e. VAL) axial load in the modelling of CSS bearings are combined with friction coefficient constant (i.e. CFC) and variable depending on sliding velocity (i.e. VFC1) and axial pressure (i.e. VFC2).

On the other hand, notable underestimation of residual displacement in the CSS bearings is obtained with the CALCFC and CALVFC1 models of the base-isolation system, especially when low-type friction properties are considered in the BIA.LF (Figure 10a) and BIB.LF (Figure 10c) structures. Variable friction coefficient with velocity (i.e. CALVFC1 model) corresponds to a decrease of residual displacement in the CSS system, in comparison with results assuming constant values of axial load and friction coefficient (i.e. CALCFC model). Moreover, a significant increase of the residual displacement is reached when variable axial load (i.e. VALCFC1 model) is taken into account, while negligible effects of friction coefficient variability with the axial pressure (i.e. VALCFC2 model) are highlighted. Finally, the inclusion of the stick-slip phases in the modelling assumptions of the CSS bearings (i.e. VALVFC3 model) can be significant, as they always induce an increase of the residual displacement.

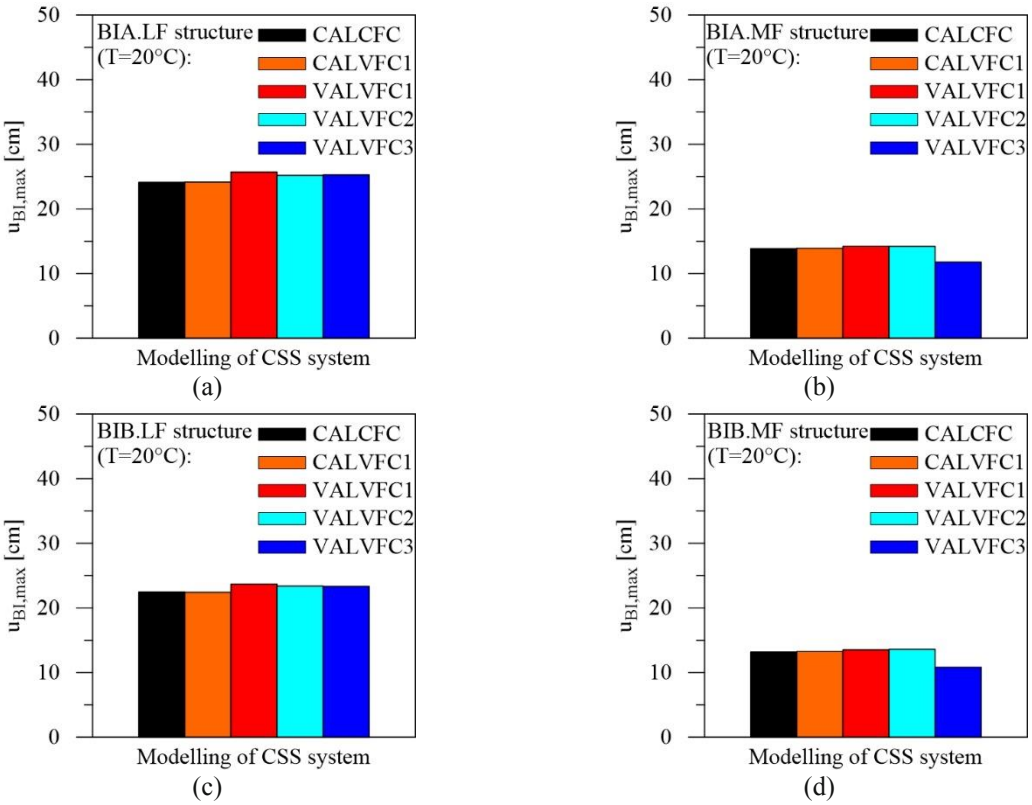

Figure 9: Effects of modelling assumptions of the CSS system on the bearing displacement.

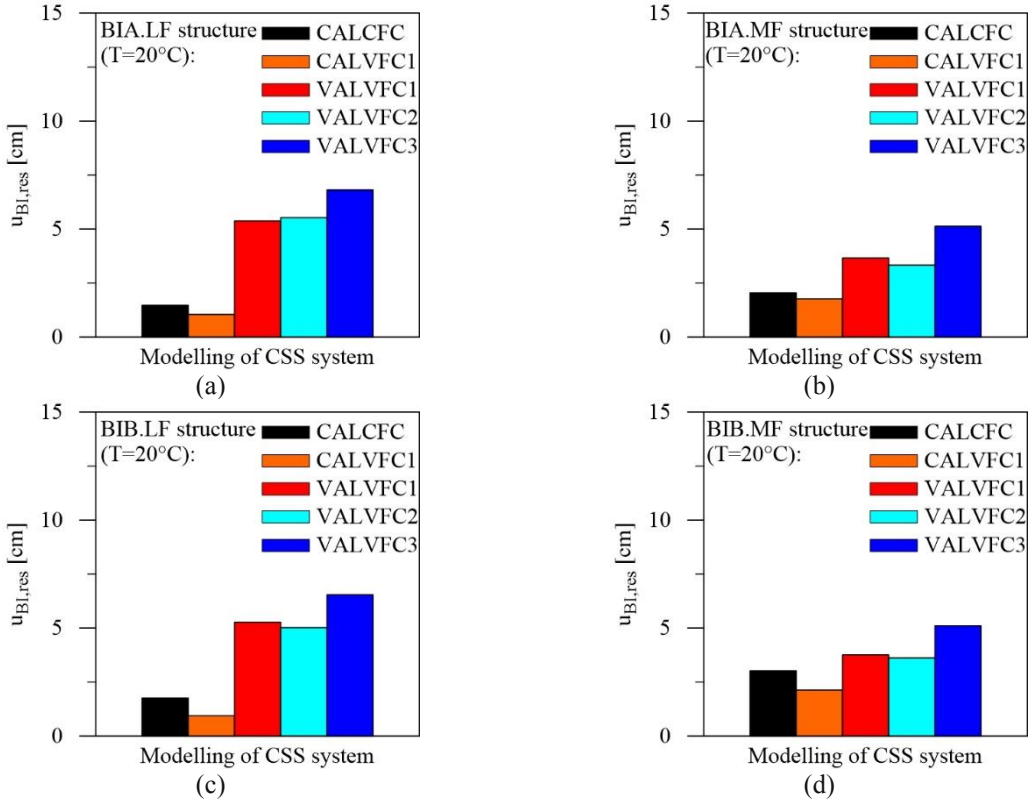

Figure 10: Effects of modelling assumptions of the CSS system on the residual bearing displacement.

Subsequently, maximum values of floor rotation at the level of the CSS system (Figure 11) highlight minor torsional effect induced by sliding velocity (i.e. CALVFC1 model) and axial pressure (i.e. VALVFC2 model), in comparison with the corresponding CSS models related

to constant values (i.e. CALCFC and VALVFC1 models). Moreover, a considerable reduction of $(tg\theta)_{BI,max}$ is found for medium-type friction properties (Figures 11b,d) when the nonlinear modelling of the CSS bearings also takes into account the sticking and sliding phases (i.e. VALVFC3 model).

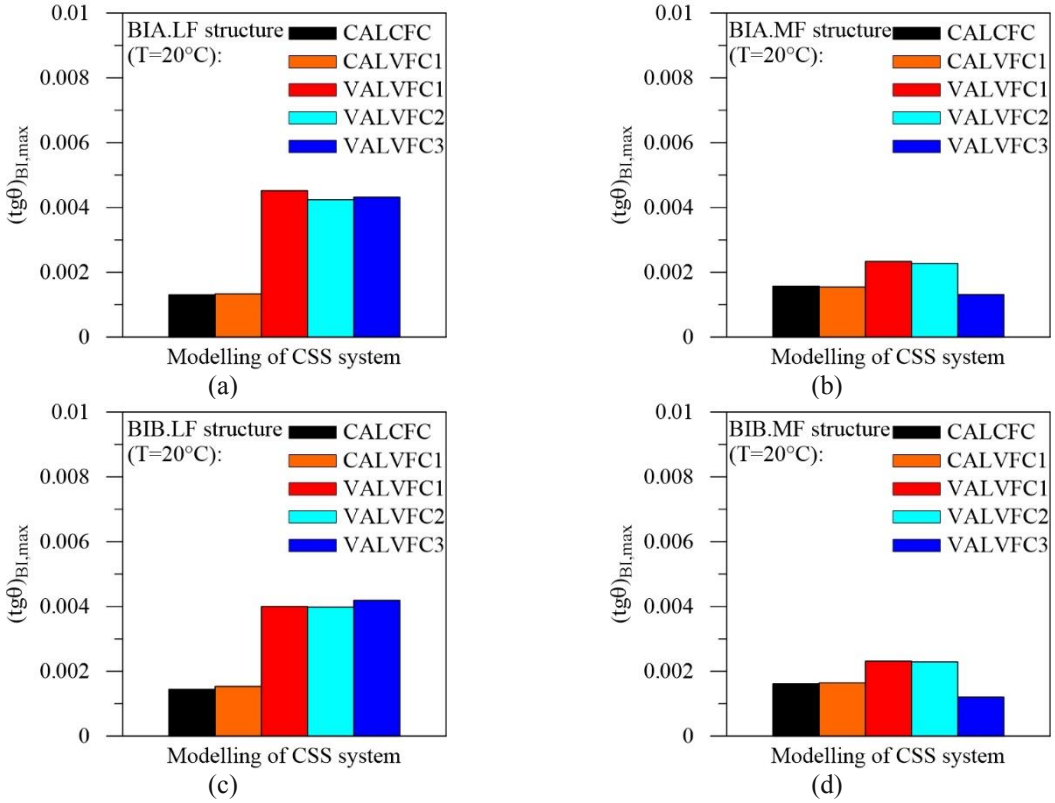

Figure 11: Effects of modelling assumptions of the CSS system on the in-plan drift ratio.

Next, in Figure 12 the sensitivity of the nonlinear seismic response parameters at the level of the CSS system is evaluated for different design and modelling assumptions of base-isolated r.c. framed buildings. To this aim, eight structural solutions are compared by considering two in-plan distributions of the dynamic-fast friction coefficient, which correspond to the same value for all isolators (i.e. the BIA structure) and a different value for each isolator (i.e. the BIB structure), and two types of friction properties (i.e. low, L, and medium, M) both evaluated in accordance with an ambient temperature T=20 °C and an increased temperature during ground motions up to T=250 °C. Moreover, the most simplified (i.e. CALCFC) and refined (i.e. VALVFC3) models of the CSS bearings are compared in Figures 12a,c,e and Figures 12b,d,f, respectively. As expected, the maximum horizontal displacement of the CSS system decreases with the change from low to medium friction properties (Figures 12a,b), but this difference becomes negligible when the heating of the CSS bearings is considered. The high temperature of the CSS bearings produces an increase of displacement which is roughly inversely proportional to the reduction factor of the friction coefficient (i.e. k_{Tf}=0.45) when medium-type friction is considered (Figure 12b). A slight increase of the horizontal displacement of the CSS system is obtained assuming the VALVFC3 model (Figure 12b) instead of the CALCFC one (Figure 12a) for both in-plan distributions of the friction coefficient. On the other hand, the residual displacement of the CSS system is affected by the modelling of the CSS system, with a marked underestimation of its value when the CALCFC model is adopted (Figure 12c). Moreover, the in-plan distribution of the friction coefficient does not produce significant changes of the residual displacement (Figures 12c,d), instead it highlights sensitiv-

ity to friction properties of the CSS bearings and reference temperature. As can be observed in Figure 12d, the highest values are those corresponding to low friction and T=250 °C (i.e. BIA.LFT and BIB.LFT structures) while the lowest ones are recorded for medium friction and T=20 °C (i.e. BIA.LF and BIB.LF structures). Note, however, that medium-type friction of the CSS bearings corresponds to less re-centring capabilities than the low-type, when expressed as a percentage of the corresponding maximum horizontal displacements.

Maximum floor rotation at the level of the CSS system proves to be sensitive to the design assumptions related to frictional heating of the CSS bearings. Specifically, the torsional effects are amplified in the case of T=250 °C and VALVFC3 model, for both low (i.e. BIA.LFT and BIB.LFT structures) and medium (i.e. BIA.MFT and BIB.MFT structures) friction-type. Moreover, the selection of medium-type friction properties produces a significant reduction of torsional effects only if the warming of the CSS bearings is ignored (i.e. assuming T=20 °C). Negligible differences among different design solutions of the CSS system are observed for the CALCFC model.

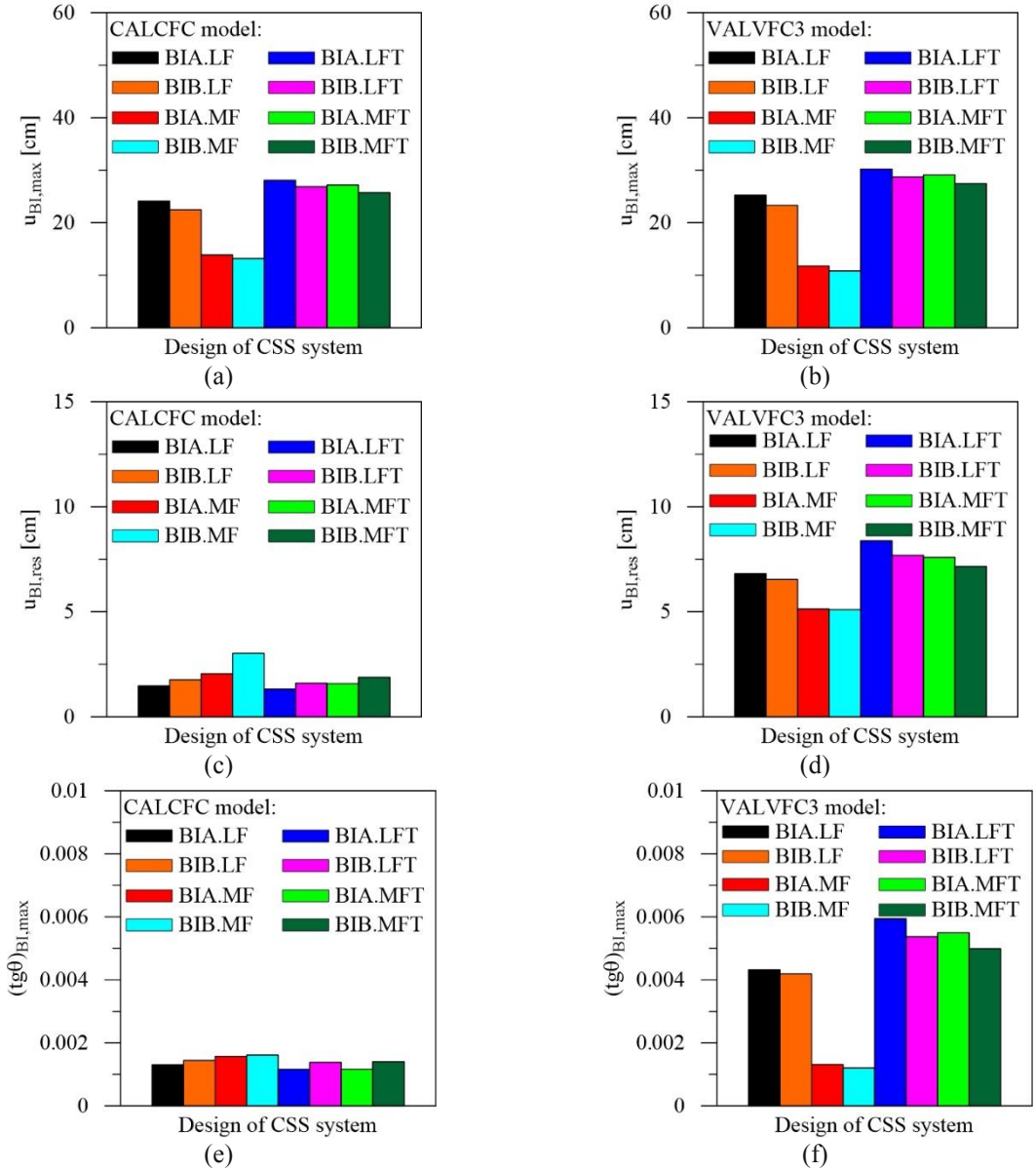

Figure 12: Effects of design assumptions of the CSS system on the response parameters.

Finally, in Figure 13 attention is focused on the sensitivity of the nonlinear seismic response of the superstructure to modelling and design assumptions of the CSS system. To this end, eight structural solutions of the CSS system are compared through the CALCFC and VALVFC3 models of the CSS bearings, while a lumped plasticity model is considered for the r.c. frame members. Maximum interstorey drift ratio $(\Delta/h)_{max}$, defined as drift normalized by storey height, is considered to represent storey damage of the superstructure. As expected, severe damage with highly irregular vertical distribution of the interstorey drift ratio is found in the case of medium friction of the CSS bearings combined with T=20 °C (i.e. BIA.MF and BIB.MF structures), especially when the VALVFC3 model is considered (Figure 13b). This behaviour can be explained by observing that for rather high values of friction the response in the horizontal direction is like that of a fixed-base structure until the friction threshold of the CSS system is not exceeded. Moreover, the other six structural solutions show light to moderate repairable damage at the storey levels and comparable results are obtained for both the CALCFC (Figure 13a) and VALVFC3 (Figure 13b) models.

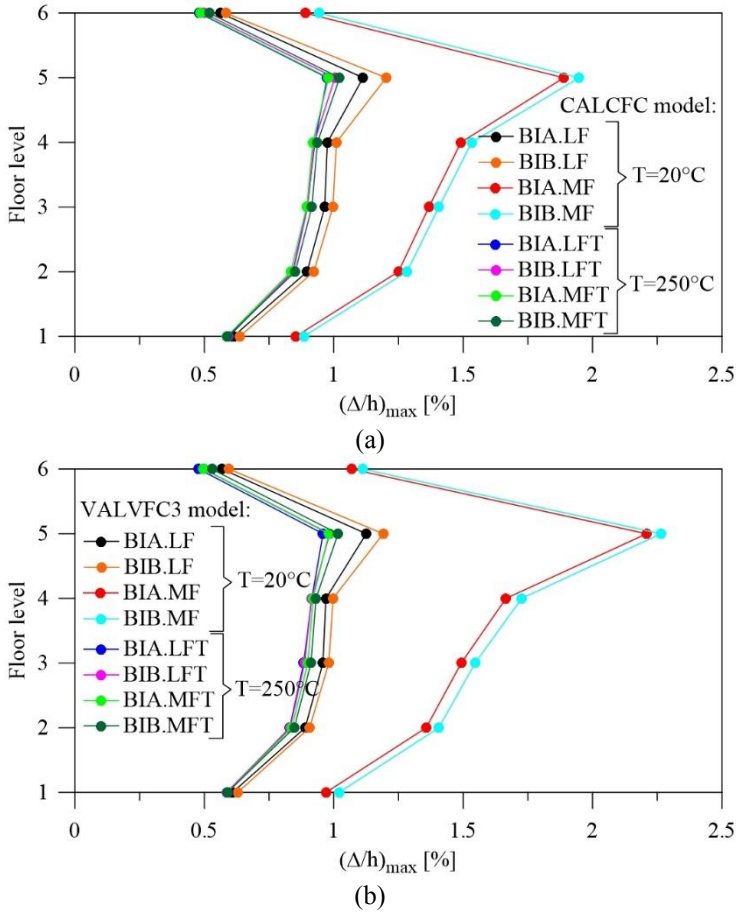

Figure 13: Effects of the modelling and design assumptions of the CSS system on the interstorey drift ratio.

5 CONCLUSIONS

The nonlinear dynamic analysis of irregular base-isolated r.c. framed structures subjected to the horizontal components of near-fault earthquakes is carried out to evaluate the effect of nonlinear modelling and seismic design of CSS bearings. Five nonlinear force-displacement laws for the CSS bearings, as function of axial load and sliding friction, are considered. Friction coefficient dependences on sliding velocity, axial pressure and stick-slip phases are also investigated. Finally, eight design solutions for the CSS system are compared to evaluate the

influence of: i) low- and medium-type friction properties; ii) two in-plan distributions of the dynamic-fast friction coefficient; iii) frictional heating at the sliding surface.

As regards the nonlinear modelling of the CSS bearings, residual displacement and floor rotation at the level of the CSS system are found to depend on the selected model, while similar values of maximum bearing displacement are obtained for all five models of CSS bearings. A significant increase in the residual displacement is reached when variable axial load (VALVFC1) and stick-slip phases (VALVFC3) are taken into account, while a considerable reduction of torsional effects occurs for medium-type friction properties when adopting the VALVFC3 model. On the other hand, maximum drift ratio of the superstructure highlights limited effects related to modelling assumptions of the CSS bearings with the only exception of medium friction of the CSS bearings combined with T=20 °C.

As regards the seismic design of the CSS system, the in-plan distribution of the friction coefficient does not produce significant changes in the demand parameters evaluated at the level of the base-isolation system. Yet, maximum horizontal displacement of the CSS system decreases with the change from low to medium friction properties, while the high temperature of the CSS bearings increases displacement. However, note that medium-type friction of the CSS bearings corresponds to less re-centring capabilities than the low-type. Finally, maximum floor rotation at the level of the CSS system proves to be sensitive to frictional heating of the CSS bearings. On the other hand, severe damage of the superstructure with highly irregular vertical distribution of the interstorey drift ratio is found in the case of medium friction of the CSS bearings and T=20 °C, while the other six structural solutions show light to moderate repairable damage. Finally, the in-plan distribution of the friction coefficient of the CSS system does not produce significant effects on the response of the superstructure.

ACKNOWLEDGEMENTS

The present work was financed by Re.L.U.I.S. (Italian network of university laboratories of earthquake engineering), in accordance with “Convenzione D.P.C.–Re.L.U.I.S. 2017, PR6 line, Isolation and Dissipation”.

REFERENCES

[1] V.A. Zayas, S.S. Low, S.A. Mahin. A simple pendulum technique for achieving seismic isolation. *Earthquake Spectra*, **6**, 317-333, 1990.

[2] M.C. Constantinou, A. Mokha, A.M. Reinhorn. Teflon bearings in base isolation. II: modeling. *Journal of Structural Engineering*, **116**(2), 455-474, 1990.

[3] P.C. Tsopelas, M.C. Constantinou, A.M. Reinhorn. 3D-BASIS-ME: computer program for nonlinear dynamic analysis of seismically isolated single and multiple structures and liquid storage tanks. *Multidisciplinary Center for Earthquake Engineering Research*, Buffalo, NY, Technical Report MCEER-94-0010, 1994.

[4] FIP Industriale S.p.A. Catalogue S04: Curved Surface Sliders. Padova, Italy. http://www.fipindustriale.it, 2013.

[5] M. Kumar, A.S. Whittaker, M.C. Constantinou. Characterizing friction in sliding isolation bearings. *Earthquake Engineering and Structural Dynamics*, **44**(9), 1409-1425, 2015.

[6] E. Fagà, P. Ceresa, R. Nascimbene, M. Moratti, A. Pavese. Modelling curved surface sliding bearings with bilinear constitutive law: effects on the response of seismically isolated buildings. *Materials and Structures*, **49**(6), 2179-2196, 2016.

[7] S. Nagarajaiah, A.M. Reinhorn, M.C. Constantinou. Torsional coupling in base isolated structures: sliding isolated systems. *ASCE/Journal of Structural Engineering*, **119**(1): 130-149, 1993.

[8] F. Mazza. Nonlinear incremental analysis of fire-damaged r.c. base-isolated structures subjected to near-fault ground motions. *Soil Dynamics and Earthquake Engineering*, **77**, 192-202, 2015.

[9] F. Mazza. Lateral-torsional response of base-isolated buildings with curved surface sliding system subjected to near-fault earthquakes. *Mechanical Systems and Signal Processing*, **92**, 64-85, 2017.

[10] Eurocode 8. Design of structures for earthquake resistance, Part1: General rules, seismic actions and rules for buildings. CEN, European Committee for Standardization, 2004.

[11] FEMA, Federal Emergency Management Agency P-751. NEHRP Recommended Seismic Provisions: Design Examples. National Earthquake Hazards Reduction Program, 2009.

[12] NTC08. Technical Regulations for the Constructions. Italian Ministry of the Infrastructures, 2008.

[13] PEER. Pacific Earthquake Engineering Research Center database. http://ngawest2.berkeley.edu, 2008.

[14] J.L. Almazan, J.C. De la Llera. Analytical model of structures with frictional pendulum isolators. *Earthquake Engineering and Structural Dynamics*, **31**, 305-332, 2002.

[15] G. Mosqueda, A.S. Whittaker, G.L. Fenves. Characterization and modeling of friction pendulum bearings subjected to multiple components of excitation. *Journal of Structural Engineering (ASCE)*, **130**(3), 433-442, 2004.

[16] J. Scheller, M.C. Constantinou. Response history analysis of structures with seismic isolation and energy dissipation systems: verification examples for program SAP2000. *Multidisciplinary Center for Earthquake Engineering Research*, State Univ. of New York at Buffalo, Buffalo, N.Y., Report No. MCEER-99-0002, 1999.

[17] M. Dolce, D. Cardone, F. Croatto. Frictional behavior of steel-PTFE interfaces for seismic isolation. *Bulletin of Earthquake Engineering*, **3**, 75-99, 2005.

[18] P.C. Roussis, M.C. Constantinou. Uplift-restraining friction pendulum seismic isolation system. *Earthquake Engineering and Structural Dynamics*, **35**, 577-593, 2006.

[19] F. Mazza, M. Mazza. Nonlinear seismic analysis of irregular r.c. framed buildings base-isolated with friction pendulum system under near-fault excitations. *Soil Dynamics and Earthquake Engineering*, **90**, 299-312, 2016.

[20] F. Mollaioli, A. Lucchini, Y. Cheng, G. Monti. Intensity measures for the seismic response prediction of base-isolated buildings. *Bulletin of Earthquake Engineering*, **11**(5), 1841-1866, 2013.

[21] F. Mazza, M. Mazza. Nonlinear analysis of spatial framed structures by a lumped plasticity model based on the Haar–Kàrmàn principle. *Computational Mechanichs*, **45,** 647-664, 2010.

[22] F. Mazza. A distributed plasticity model to simulate the biaxial behaviour in the nonlinear analysis of spatial framed. *Computers and Structures*, **135**, 141-154, 2014.